Research Article

Thermal lens study of absolute porosity in ceria: A Sankar–Loeb model approach

Riya Sebastian[1] · M. S. Swapna[1] · S. Sankararaman[1]

Abstract

The present work divulges the potential of thermal lens technique for analyzing the absolute porosity of a material in nanofluid using the recently proposed Sankar–Loeb model. The ceria nanoparticles synthesized by co-precipitation technique are subjected to morphological and structural characterizations. The study reveals that particle size and thermal diffusivity increase with annealing temperature. The nanocavities formed during the agglomeration of nanoparticles result in closed pores which give rise to absolute porosity that is probed by the thermal wave propagation (or thermal diffusivity) study. The enhancement in the particle size enhances the closed pore volume in the sample resulting in increased absolute porosity. Thus, the TL technique makes the analysis of closed pores possible through the absolute porosity study, which is not possible with the conventional BET (Brunauer–Emmett–Teller) technique.

Keywords Absolute porosity · Sankar–Loeb model · Ceria nanofluid · Thermal lens technique

1 Introduction

The advancement in nanoscience and nanotechnology led to the development of novel materials for diversified industrial applications during the last two decades. An understanding of thermal properties of materials is essential for its electronic and photonic applications [1–3]. The low thermal conductivity of traditional heat transfer fluids can be improved by making nanofluids with nanometer-sized particles in base fluids. Since nanoparticles have a high surface-to-volume ratio, they can stay suspended for a long time compared to large-sized particles [4]. So, these multicomponent liquids with nanosized particles as the suspended particles show good thermal conductivity. Because of this reason, nanofluids have emerged as a new class of material, for efficient heat transfer, finding a wide range of industrial applications [5, 6]. The thermal, electrical and electronic property of a material at the nanoscale is greatly influenced by the porosity in it [1, 7]. Nanoporous materials have emerged as potential materials exhibiting

promising dielectric, thermoelectric and electronic properties that led to the development of large-scale integrated circuits and thermoelectric devices to converting heat to electricity [1, 8]. Today we have porous ceramics metallic foams and composite materials finding a variety of applications in fields like biochemical and electrochemical engineering, medicine and hydrology. The flow of fluid (single/two phase—gas or/and liquid) through the interconnected voids (pores) is found to be affected by the varying size and shape of the pores [9, 10]. Thus, by designing nanoporous materials of varying shape, size and number density of pores, the physical and thermal properties of the material can be tailored.

Nanofluids are commonly prepared by dispersing nanoparticles of metal, non-metal, ceramics and metal oxides in the base fluids water, ethanol and oil [11–13]. In the present work, CeO_2 nanoparticles are selected for preparing the CeO_2-ethanol nanofluid. CeO_2 is a vital material finding a wide range of applications in capacitors, electrolyte material in fuel cells, UV blocks, buffer layers for conductors,

✉ S. Sankararaman, drssraman.opto@gmail.com | [1]Department of Optoelectronics, University of Kerala, Trivandrum, Kerala 695581, India.

polishing materials, thermal barrier coating and coating in optical device. The importance of ceria is due to its unique features like biocompatibility, nontoxicity, electrocatalytic ability, oxygen storage capability, thermal and optical properties [12–15].

The thermal conductivity of the nanofluid dramatically depends on the factors like morphology of the particle, size and shape of the particle, energy flux, physical properties [16] of the base fluid, etc. Some theoretical models are put forward by researchers like Choi et al. [12], Wang et al. [17], Maxwell-Garnet, Keblinski et al. [18], Yu and Choi [19], Patel et al. [20] and Mehta et al. [21], for explaining the thermal conductivity of nanofluids. However, these models are not capable of explaining the thermal behaviour entirely and satisfactorily [20]. So, recently, a model named as Sankar–Loeb model of generalized theory of thermal conductivity is developed which can successfully be applied in the case of liquids, solids and nanofluids. This model helps in understanding the thermal behaviour of nanofluids with porous/heterogenous/homogenous/core–shell materials. The model considers only the closed pores in defining the absolute porosity, while all other structures (non-closed) are considered as irregular shaped particles. The absolute porosity is defined as the ratio of total extent of closed porous region in the direction of heat propagation to the length of the sample. The morphological modifications and porosity of the material can also be analyzed by using this theory [22]. So, in this work, the Sankar–Loeb model is used for analyzing the effect of nanocavities region in CeO_2 on the thermal diffusivity of CeO_2-ethanol nanofluid.

Of several methods of thermal characterization of nanofluids under steady-state conditions, laser-based thermal lens technique (TLT) offers high sensitive, nondestructive and transient heat flow analysis in the determination of thermal diffusivity of nanofluids [11]. The technique involves the analysis of refractive index gradient produced within the medium as a result of optical absorption and subsequent nonradiative deexcitation. The nature of the thermal lens (TL) formed depends on the thermal diffusivity of a medium. Compared to conventional spectroscopic techniques, TLT is capable of sensing thermal energy variation $\sim 10^{-6}$ J to 10^{-4} J, as only the absorbed photons contribute to the TL signal, and this makes the technique suitable for the studies related to trace detection, quantum yield and reaction kinetics [23].

2 Materials and method

2.1 Experimental

The commonly used chemical methods for the synthesis of nanoparticles are solgel technique, hydrolysis, condensation,

growth and agglomeration, and co-precipitation [24, 25]. In the present work, the ceria nanoparticles are synthesized by co-precipitation technique as it provides greater control over its physical properties. In the present work for the synthesis of ceria, 0.1 M cerium nitrate and ammonium carbonate solutions are prepared in double-distilled water. Freshly prepared ethylenediaminetetraacetic acid (EDTA) solution is added dropwise with stirring to the cerium nitrate solution, which is then added dropwise to the ammonium carbonate solution under constant stirring. The stirring is continued for half an hour. The resultant pale yellow coloured precipitate is then centrifuged and washed out with distilled water five times for removing water-soluble undesired by-products and impurities [26]. The dried precipitate is then calcined at 400 °C, 550 °C, 700 °C and 850 °C. They are labelled as S1, S2, S3 and S4, respectively. The samples are subjected to morphological characterization using Nova Nano Field Emission Scanning Electron Microscopic (FESEM). The structural characterizations are done with X-ray diffractometer (Bruker D8 Advanced) with CuKα radiation ($\lambda = 1.5406$ Å) and Fourier transform infrared spectroscopy (FTIR) with Shimadzu IR Affinity—1 FTIR spectrophotometer.

2.2 Thermal lens study

The ceria nanofluids are prepared by dispersing 2 mg ceria (S1–S4) in 4 ml ethanol. The thermal diffusivity (α) variation of the nanofluids is studied using the single-beam thermal lens arrangement shown in Fig. 1. The experimental set up consists of a He–Cd continuous wave (CW) laser of 442 nm wavelength and power 80 mW. The laser beam is intensity modulated using an electromechanical chopper operating at 2 Hz and focused by a convex lens of 20 cm focal length on to the sample taken in the quartz cuvette. At the focal point, the beam spot size (ω) is calculated to be 0.11 ± 0.01 mm. The focal length of the TL thus formed is given by

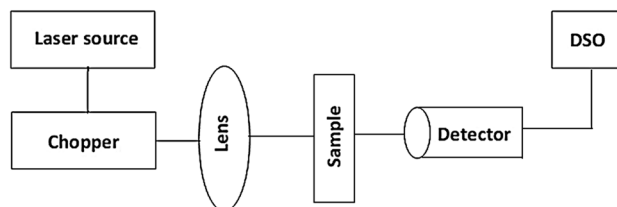$$f(t) = f(\infty)\left(1 + \frac{t_c}{2t}\right) \tag{1}$$

Fig. 1 Schematic representation of single-beam thermal lens technique

where $f(\infty)$ and t_c represent the steady-state focal length and the characteristic time constant, respectively, from which α can be calculated using the relation [27]

$$\alpha = \frac{\omega^2}{4t_c} \quad \text{in m}^2/\text{s} \tag{2}$$

The emergent beam from the sample is collected using an optical fiber and detected using a sensitive photodetector. The output of the photodetector is fed to a Digital Storage Oscilloscope (DSO 500 MHz). The emergent beam intensity at time t ($I(t)$) is given by [28]

$$I(t) = I_0 \left[1 - \theta \left(1 + \frac{t_c}{2t} \right)^{-1} + \frac{1}{2}\theta^2 \left(1 + \frac{t_c}{2t} \right)^{-2} \right]^{-1} \tag{3}$$

where I_0 and θ denote the initial beam intensity and a parameter related to photothermal energy, respectively. A MATLAB program is used for curve fitting the TL signal recorded in the DSO using Eq. (3) to get the value of t_c from which α is calculated using Eq. (2). The standardization of the experimental setup is done by finding the value of α for water ($1.41 \times 10^{-7} \pm 0.01$ m^2/s), which is in agreement with the literature [29].

2.3 Sankar–Loeb model of thermal conductivity

In the present study, Sankar–Loeb model of thermal conductivity is adopted for analyzing the thermal diffusivity of different samples. According to this model, in the case of nanofluids, there occurs a laminar heat flow through the medium (Fig. 2a). So, the total length of the sample can be written as [22]

$$L = \sum \Delta x_l + \sum \Delta x_s + \sum \Delta x_p = l + l_s + l_p \tag{4}$$

where l_s: total length of the solid portion $= \sum \Delta x_s$, l: total length of the liquid portion $= \sum \Delta x_l$ and l_p: total length of the porous portion of the closed pores $= \sum \Delta x_p$.

The Sankar–Loeb equation connects the effective thermal conductivity (k_{eff}) of the medium and absolute porosity $\left(P = \frac{l_p}{L} \right)$ by the relation [22]

$$\frac{1}{k_{eff}} = (1 - P)\left(\frac{1}{k_l} + \frac{1}{k_s} \right) - \left(\frac{l_s}{Lk_l} + \frac{l}{Lk_s} \right) + \frac{n_p}{4L\gamma e \sigma T^3} \tag{5}$$

where k_l is the thermal conductivity of the liquid, k_s is the thermal conductivity of the solid, n_p is the number of pores, γ is the geometrical shape factor, T is the average absolute temperature at the porous region, e is the emissivity of the radiating surface and σ is the Stefan's radiation constant.

According to Sankar–Loeb model, P in Eq. (5) represents the absolute porosity accounting the closed pores and all other structures (non-closed) are considered as irregular shaped particles [22].

Neglecting the higher-order terms, Eq. (5) becomes

$$\frac{1}{k_{eff}} = (1 - P)\left(\frac{1}{k_l} + \frac{1}{k_s} \right) \tag{6}$$

or

$$\frac{k_l}{k_{eff}} = (1 - P)\left(1 + \frac{k_l}{k_s} \right) \tag{7}$$

When the size of the closer pore (l_p) increases, the particle size also increases. This, in turn, increases the total length of heat propagation through the solid portion, which is responsible for the increase in the effective thermal conductivity (k_{eff}) of the nanofluid. For nonporous nanoparticles dispersed in the liquid medium, Eq. (5) becomes [22]

$$\frac{1}{k_{eff}} = \left(\frac{1}{k_l} + \frac{1}{k_s} \right) - \left(\frac{l_s}{Lk_l} + \frac{l}{Lk_s} \right) \approx \left(\frac{1}{k_l} + \frac{1}{k_s} \right) - \frac{l_s}{Lk_l} \tag{8}$$

This clearly reveals the increase in the value of k_{eff} with particle size.

Fig. 2 (**a**) Representation of laminar heat flow through the medium. (**b**) Representation of nanocavities between nanoparticles
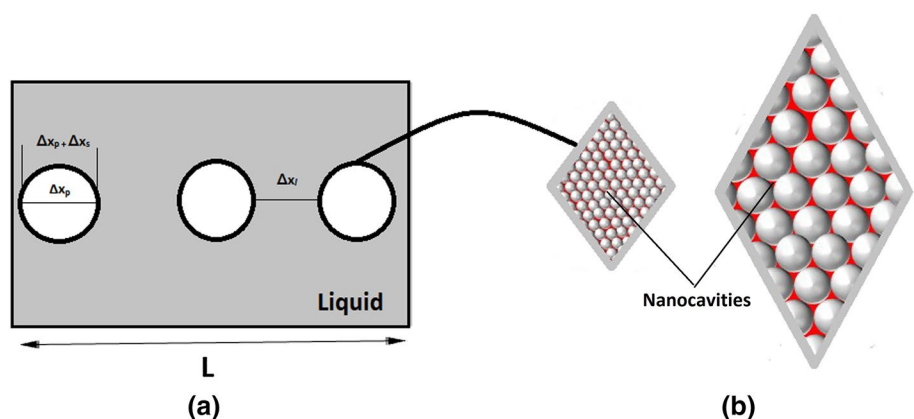
3 Results and discussion

The morphological modifications of ceria upon annealing are understood from the FESEM images shown in Fig. 3, which shows that the agglomeration of ceria nanoparticles increases with annealing temperature. The enlarged image of a portion of Fig. 3d shown in the inset clearly reveals the formation of the bigger particle as a result of the agglomeration of smaller particles, which itself is the agglomeration of ceria nanoparticles.

The X-ray diffraction (XRD) pattern of the samples S1–S4 recorded with a scanning step of 0.02° in the range of $2\theta = 10°–80°$ is shown in Fig. 4. From the comparison of peaks in the XRD pattern with the JCPDS file, no 75–0076 reveals that the structure of the ceria synthesized is face-centered cubic. The XRD pattern of S1 shows the characteristic peaks around 28.5°, 33°, 47° and 56° corresponding to the planes (111), (200), (220) and (311), respectively. When the sample is calcined at 550 °C (S2) in addition to the peaks in the XRD pattern of S1, some more additional peaks of ceria become visible around 59°, 69°, 76° and 79° corresponding to the planes (222), (400), (331) and (420), respectively. Figure 4 shows a further enhancement of the intensity of these characteristic peaks of ceria with a reduction in full width at half maximum (FWHM-β) with the increase in annealing temperature. From the calculation of average particle size (τ) using the Scherrer equation, $\tau = 0.9\lambda/\beta \cos\theta$ [30], it is evident that the average particle size increases with the annealing temperature, which
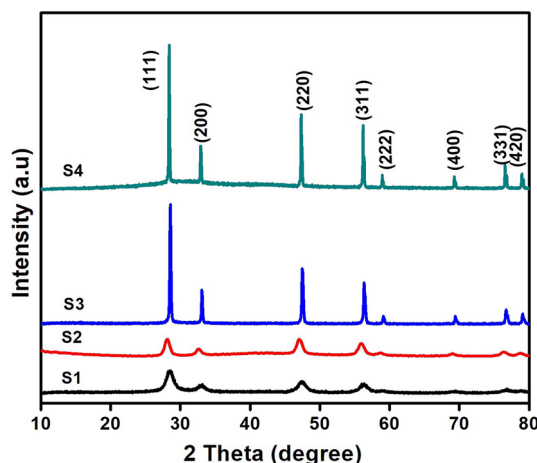

Fig. 4 XRD pattern of the ceria samples calcined at 400 °C—S1, 550 °C—S2, 700 °C—S3 and 850 °C—S4

is in agreement with the literature [16]. The variation of average particle size with the annealing temperature is shown in Fig. 5.

The structure of the sample can be understood from the Fourier transform infrared (FTIR) spectroscopy shown in Fig. 6. The FTIR spectrum recorded in the range 400–4000 cm^{-1} for the samples S1–S4 shows the signature peaks of Ce–O stretching vibrations around 450 cm^{-1} and 845 cm^{-1} [26, 31]. Other peaks in the FTIR spectrum and their assignments [26, 31–35] are given in Table 1.

Fig. 3 FESEM images of ceria samples calcined at (**a**) 400 °C—S1, (**b**) 550 °C—S2, (**c**) 700 °C—S3 and (**d**) 850 °C – S4
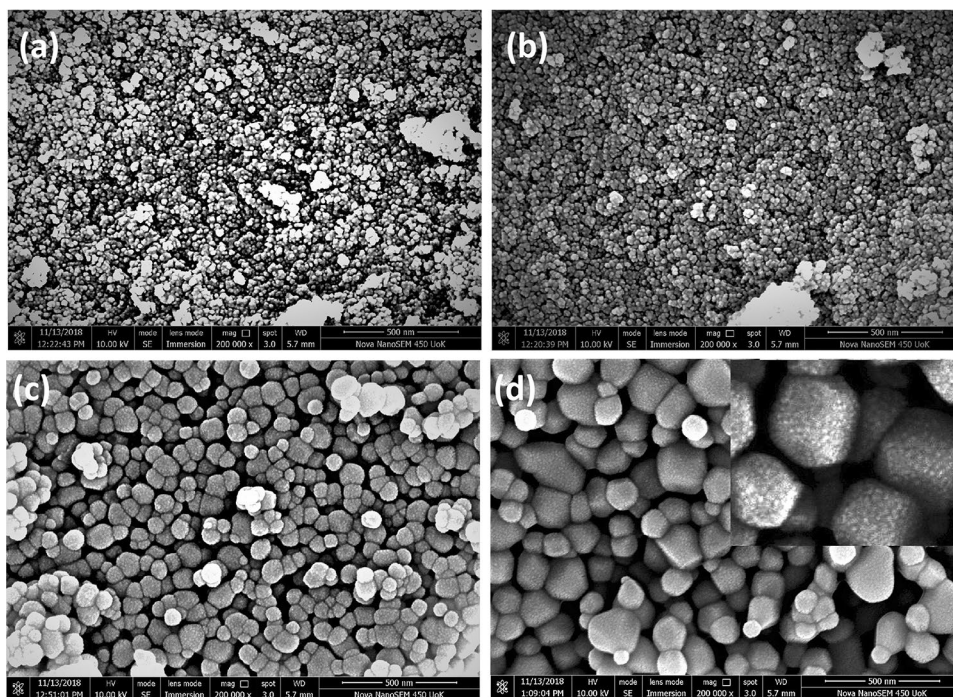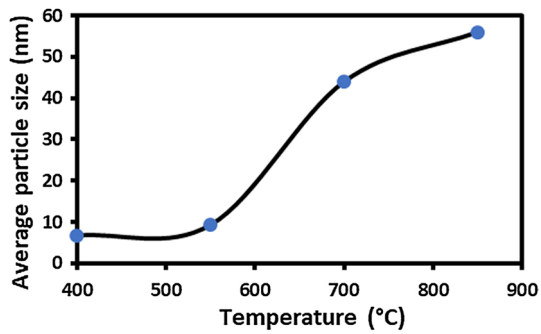
Fig. 5 Variation of average particle size of ceria samples with temperature

The percentage variation of thermal diffusivity of ceria nanofluid is shown in Fig. 7. The ceria samples (S1–S4) with varying particle size, due to annealing at different temperatures, are found to enhance the thermal diffusivity of the base fluid, ethanol. It is well reported in the literature that the thermal diffusivity depends on factors like the nature of the base fluid, shape and size of the nanoparticle [17]. When the particle size increases, the total length of heat propagation through the solid portion also increases which is responsible for the increase in the effective

thermal conductivity (k_{eff}) of the nanofluid as envisaged by the theoretical model. The observed increase in thermal diffusivity of the sample (with a standard error $\pm 0.01 \times 10^{-7}$ m^2/s) and the percentage enhancement, shown in Fig. 7, for the nanofluid with samples S1–S4 is in good agreement with the Sankar–Loeb model.

Of various methods of porosity analysis, BET (Brunauer–Emmett–Teller) method is the most commonly used. However, this technique has the limitation that it depends on gas adsorption by a surface and hence not sensitive to closed surfaces [36]. The results from BET method are accurate for materials with large pore surface area, suitable adsorbent and uniform adsorption of gas molecules without interaction. Thus, for pores of smaller surface area and poor adsorbents of gas molecules, a precise quantitative analysis of porosity is difficult with BET technique. The application of Sankar–Loeb model removes this limitation and enables to study the absolute porosity through thermal diffusivity measurements using single-beam thermal lens technique. During the formation of the bigger particle as a result of the agglomeration of smaller particles, which itself is the agglomeration of ceria nanoparticles, lot of nanocavities (as in Fig. 2b) get introduced. These nanocavities give a porous structure to the sample, the absolute porosity

Fig. 6 FTIR spectra of ceria samples calcined at (**a**) 400 °C—S1, (**b**) 550 °C—S2, (**c**) 700 °C—S3 and (**d**) 850 °C—S4
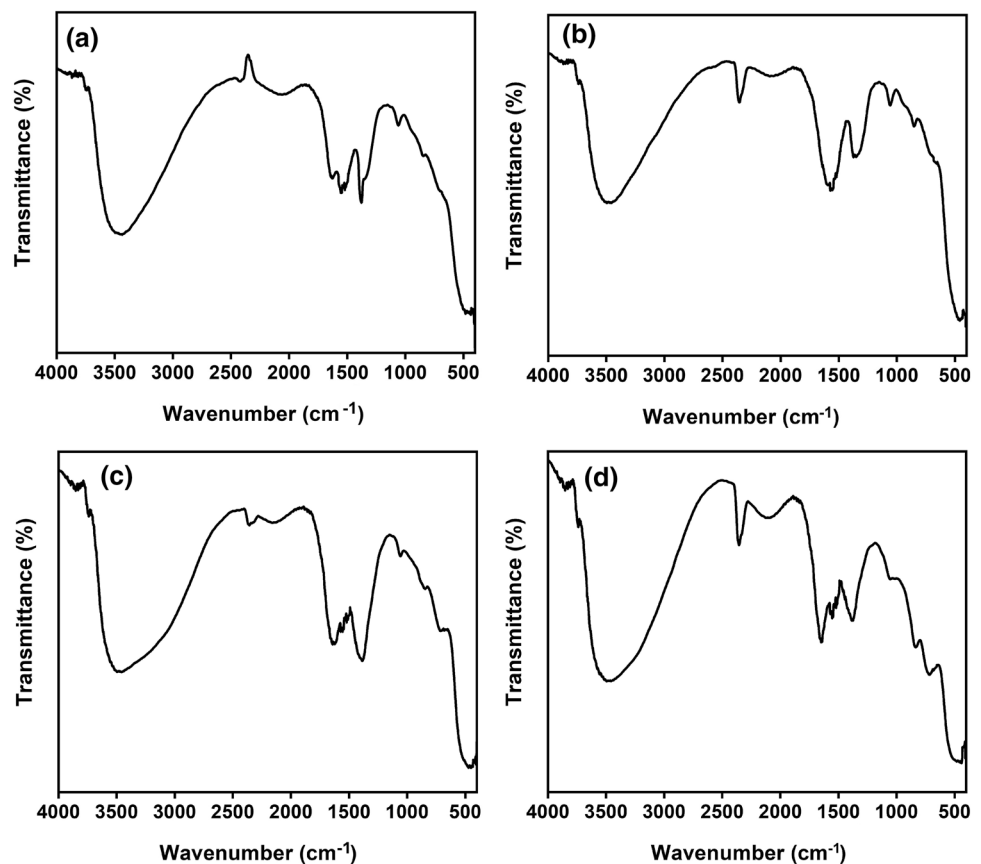
Table 1 Peak assignments of FTIR spectra

Wavenumber (cm⁻¹)				Assignment
S1	S2	S3	S4	
455	458	454	478	Ce–O stretching vibration
847	853	846	835	Ce–O stretching vibration
1059	1057	1059	1054	C–O stretching vibration
1377	1372	1384	1381	Physically adsorbed water molecule
1552	1553	1552	1551	Bending vibration of water molecule
1629	1638	1639	1647	Bending vibration of water molecule
3456	3477	3496	3486	Physically adsorbed water molecule

of which can be measured easily and accurately by this method. Figure 5 shows that the effect of annealing is to enhance the particle size. From the theoretical model and literature [16], it is well known that the thermal diffusivity (or conductivity) increases with particle size. The variation of thermal diffusivity with particle size is shown in Fig. 8a. The variation of absolute porosity with sample annealing temperature and thermal diffusivity is shown in Fig. 8b and c. The increase in absolute porosity with

annealing temperature (Fig. 8b) is due to the increase in particle size as a result of the expansion of nanocavities.

4 Conclusion

The present work reports a method to find the absolute porosity of a material through thermal diffusivity study using the sensitive and nondestructive TL technique employing the recently proposed Sankar–Loeb model. Study of porosity in materials is highly significant as it influences the physical and chemical properties of it. In this work, porous ceria nanoparticles are synthesized by co-precipitation technique and its morphological and structural characterizations are carried out with FESEM, XRD and FTIR techniques. The study reveals that the absolute porosity increases with thermal diffusivity, which in turn is found to increase with the increase in particle size. It is also observed that the annealing temperature modifies the nanocavities in such a way that the size of the agglomerated particle increases. The work also suggests the advantage of application of the TL technique along
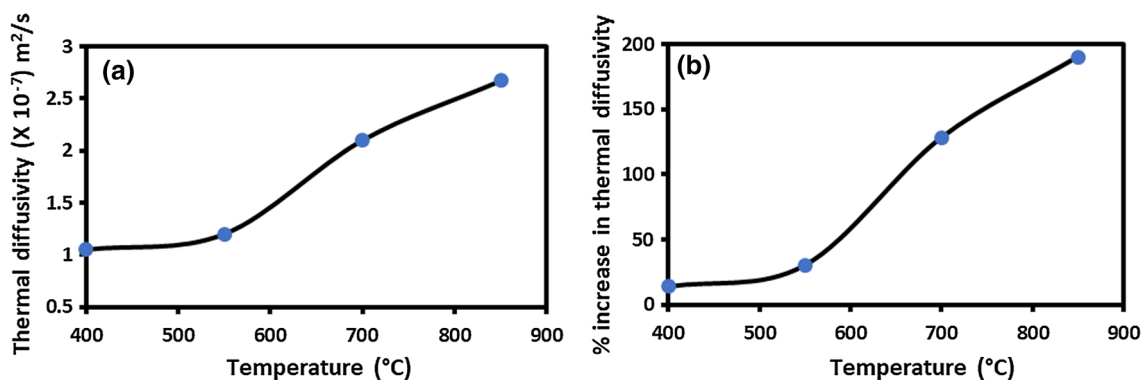
Fig. 7 (**a**) Variation in thermal diffusivity of ceria nanofluid with temperature. (**b**) Percentage increase in the thermal diffusivity of ceria nanofluid with temperature
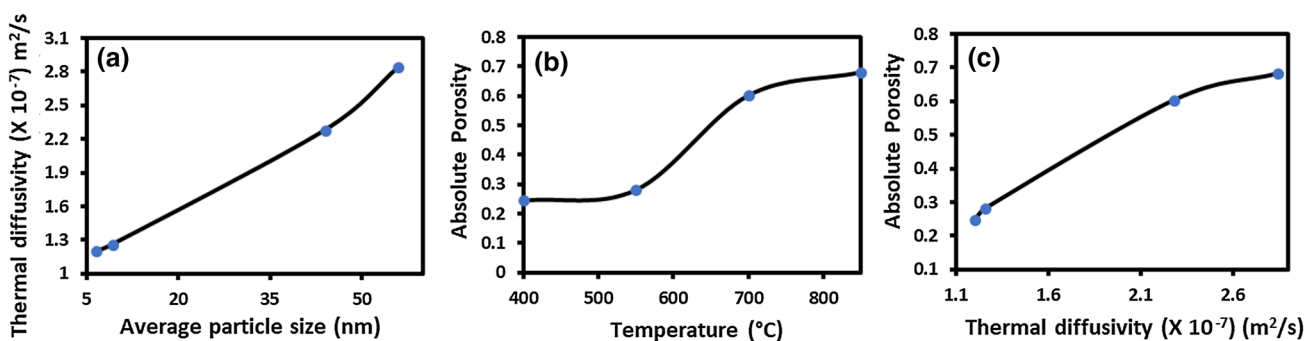
Fig. 8 Variation of (**a**) thermal diffusivity with average particle size, (**b**) absolute porosity with sample annealing temperature and (**c**) absolute porosity with thermal diffusivity

with Sankar–Loeb model to study the variation of absolute porosity, instead of using BET analysis. The TL technique described in this paper complements the limitation of BET technique as it accounts closed pores. Thus, the TL technique can be used as a potential tool for porosity analysis.

Compliance with ethical standards

Conflict of interest The authors declare that they have no conflict of interest.

References

1. Sumirat I, Ando Y, Shimamura S (2006) Theoretical consideration of the effect of porosity on thermal conductivity of porous materials. J Porous Mater 13:439–443
2. Schlichting KW, Padture NP, Klemens PG (2001) Thermal conductivity of dense and porous yttria-stabilized zirconia. J Mater Sci 36:3003–3010
3. Zhao K, Qiu P, Song Q, Blichfeld AB, Eikeland E, Ren D et al (2017) Ultrahigh thermoelectric performance in Cu_2–ySe0.5S0.5 liquid-like materials. Mater Today Phys 1:14–23
4. Colangelo G, Favale E, de Risi A, Laforgia D (2012) Results of experimental investigations on the heat conductivity of nanofluids based on diathermic oil for high temperature applications. Appl Energy 97:828–833
5. Eastman JA, Phillpot SR, Choi SUS, Keblinski P (2004) Thermal transport in nanofluids. Annu Rev Mater Res 34:219–246
6. Tuckerman DB, Pease RFW (1981) High-performance heat sinking for VLSI. IEEE Electron Device Lett 2:126–129
7. Roberts JN, Schwartz LM (1985) Grain consolidation and electrical conductivity in porous media. Phys Rev B 31:5990
8. Tarkhanyan RH, Niarchos DG (2013) Reduction in lattice thermal conductivity of porous materials due to inhomogeneous porosity. Int J Therm Sci 67:107–112
9. Dullien FAL (2012) Porous media: fluid transport and pore structure. Academic press, USA
10. Nield DA, Bejan A (2006) Convection in porous media. Springer, New York
11. Singh AK (2008) Thermal conductivity of nanofluids. Def Sci J 58:600–607
12. Choi SUS (2008) Nanofluids: a new field of scientific research and innovative applications. Taylor & Francis 29:429–431
13. Saleh R, Putra N, Wibowo RE, Septiadi WN, Prakoso SP (2014) Titanium dioxide nanofluids for heat transfer applications. Exp Therm Fluid Sci 52:9–29
14. Brandon JR, Taylor R (1989) Thermal properties of ceria and yttria partially stabilized zirconia thermal barrier coatings. Surf Coat Technol 39:143–151
15. Miller RA (1987) Current status of thermal barrier coatings—an overview. Surf Coat Technol 30:1–11
16. Sebastian R, Swapna MS, Raj V, Hari M, Sankararaman S (2018) Thermal diffusivity control in titanium dioxide nanofluid through phase tuning. Mater Res Express 5:75001
17. Wang BX, Zhou LP, Peng XF (2003) A fractal model for predicting the effective thermal conductivity of liquid with suspension of nanoparticles. Int J Heat Mass Transf 46:2665–2672
18. Angayarkanni SA, Philip J (2015) Review on thermal properties of nanofluids: recent developments. Adv Colloid Interface Sci 225:146–176
19. Yu W, Choi SUS (2003) The role of interfacial layers in the enhanced thermal conductivity of nanofluids: a renovated Maxwell model. J Nanoparticle Res 5:167–171
20. Patel HE, Sundararajan T, Das SK (2008) A cell model approach for thermal conductivity of nanofluids. J Nanoparticle Res 10:87–97
21. Mehta S, Chauhan KP, Kanagaraj S (2011) Modeling of thermal conductivity of nanofluids by modifying Maxwell's equation using cell model approach. J Nanoparticle Res 13:2791–2798
22. Swapna MS, Sankararaman S (2019) Generalized theory of thermal conductivity for different media: solids to nanofluids. J Phys Chem C 123:23264–23271
23. Raj V, Swapna MS, Saritha Devi HV, Sankararaman S (2019) Non-radiative analysis of adulteration in coconut oil by thermal lens technique. Appl Phys B 125:113
24. Rajput N (2015) Methods of preparation of nanoparticles-a review. Int J Adv Eng Technol Citeseer 7:1806
25. Bader N, Zimmermann BAAB (2014) Co-precipitation as a sample preparation technique for trace element analysis: an overview. Int J Chem Sci 12:519–525
26. Babitha KK, Sreedevi A, Priyanka KP, Sabu B, Varghese T (2015) Structural characterization and optical studies of CeO2 nanoparticles synthesized by chemical precipitation. Indian J Pure Appl Phys 53:596–603
27. Gordon JP, Leite RCC, Moore R, Porto SPS, Whinnery JR (1965) Long-transient effects in lasers with inserted liquid samples. J Appl Phys 36:3–8
28. Hu C, Whinnery JR (1973) New thermooptical measurement method and a comparison with other methods. Appl Opt 12:72–79
29. Abramson EH, Brown JM, Slutsky LJ (2001) The thermal diffusivity of water at high pressures and temperatures. J Chem Phys 115:10461–10463
30. Stokes AR, Wilson A J C (1942) A method of calculating the integral breadths of Debye–Scherrer lines. Math Proc Cambridge Philos Soc, Cambridge University Press 313–22
31. Goharshadi EK, Samiee S, Nancarrow P (2011) Fabrication of cerium oxide nanoparticles: characterization and optical properties. J Colloid Interface Sci 356:473–480
32. Yang H, Huang C, Tang A, Zhang X, Yang W (2005) Microwave-assisted synthesis of ceria nanoparticles. Mater Res Bull 40:1690–1695
33. Khadar YAS, Balamurugan A, Devarajan VP, Subramanian R, Kumar SD (2018) Synthesis, characterization and antibacterial activity of cobalt doped cerium oxide (CeO2:Co) nanoparticles by using hydrothermal method. J Mater Res Technol 8:267–274
34. Sahoo SK, Mohapatra M, Singh AK, Anand S (2010) Hydrothermal synthesis of single crystalline nano CeO2 and its structural, optical, and electronic characterization. Mater Manuf Process 25:982–989
35. Shahriari E, Yunus WMM, Zamiri R (2013) The effect of nanoparticle size on thermal diffusivity of gold nano-fluid measured using thermal lens technique. J Eur Opt Soc Publ 8:13026
36. Ambroz F, Macdonald TJ, Martis V, Parkin IP (2018) Evaluation of the BET theory for the characterization of meso and microporous MOFs. Small Methods 2:1800173